AGU ADVANCING EARTH AND SPACE SCIENCE

Geophysical Research Letters®

RESEARCH LETTER
10.1029/2021GL097525

Key Points:

- We investigate the influence of solid Earth deformation on the contribution of the Antarctic Ice Sheet to projections of sea-level change
- The water outflux from uplifting flooded marine basins adds to future projections by up to 16% at the end of the 21st century and 14% at 2500
- Not incorporating the 3-D Earth structure underestimates the geographically variable far-field sea-level by up to 20% at the end of the simulations (2500)

Supporting Information:

Supporting Information may be found in the online version of this article.

Correspondence to:

M. Yousefi,
maryam.yousefi@mcgill.ca

Citation:

Yousefi, M., Wan, J., Pan, L., Gomez, N., Latychev, K., Mitrovica, J. X., et al. (2022). The influence of the solid Earth on the contribution of marine sections of the Antarctic Ice Sheet to future sea-level change. *Geophysical Research Letters*, *49*, e2021GL097525. https://doi.org/10.1029/2021GL097525

Received 4 JAN 2022
Accepted 6 JUL 2022

The Influence of the Solid Earth on the Contribution of Marine Sections of the Antarctic Ice Sheet to Future Sea-Level Change

M. Yousefi[1,2], J. Wan[1], L. Pan[3], N. Gomez[1], K. Latychev[3], J. X. Mitrovica[3], D. Pollard[2], and R. M. DeConto[4]

[1]Department of Earth and Planetary Sciences, McGill University, Montreal, QC, Canada, [2]Earth and Environmental Systems Institute, Pennsylvania State University, University Park, PA, USA, [3]Department of Earth and Planetary Sciences, Harvard University, Cambridge, MA, USA, [4]Department of Geosciences, University of Massachusetts Amherst, Amherst, MA, USA

Abstract Seismic tomography models indicate highly variable Earth structure beneath Antarctica with anomalously low shallow mantle viscosities below West Antarctica. An improved projection of the contribution of the Antarctic Ice Sheet to sea-level change requires consideration of this complexity to precisely account for water expelled into the ocean from uplifting marine sectors. Here we build a high-resolution 3-D viscoelastic structure model based on recent inferences of seismic velocity heterogeneity below the continent. The model serves as input to a global-scale sea-level model that we use to investigate the influence of solid Earth deformation in Antarctica on future global mean sea-level (GMSL) rise. Our calculations are based on a suite of ice mass projections generated with a range of climate forcings and suggest that water expulsion from the rebounding marine basins contributes 4%–16% and 7%–14% to the projected GMSL change at 2100 and 2500, respectively.

Plain Language Summary Most of vulnerable sections of the Antarctic Ice Sheet rests on top of bedrock below sea level and the bed deepens inland. Following the ice loss in these sections, the underlying bedrock rebounds and expels the meltwater into the open ocean, a process that is called water expulsion. The impact of this mechanism on future estimates of sea-level change has not been fully investigated. Here, we project the effect of water expulsion mechanism on geographically variable global sea-level change.

1. Introduction

There is substantial uncertainty in the contribution of the Antarctic Ice Sheet (AIS) to future global mean sea-level (GMSL) rise mainly due to the relatively poor constraints on the processes and feedbacks that lead to its mass loss (DeConto et al., 2021; Pattyn & Morlighem, 2020; Seroussi et al., 2020). The processes that cause ice sheet instability are sensitive to the characteristics of the underlying bed, including its slope, roughness, elevation and how it deforms. Published bathymetric maps of Antarctica reveal that about a third of this ice sheet lies on top of bedrock that is considerably below sea level (e.g., Fretwell et al., 2013; Morlighem et al., 2019). A combination of the negative bedrock elevation, reverse-sloping beds, and warming climate provides a positive feedback on ice retreat which can trigger marine ice sheet instability (MISI) (e.g., Schoof, 2007). In addition, a marine ice cliff instability (MICI) has been proposed, which enhances the ice loss in marine basins. This process involves ice shelf breakup driven by crevasse penetration enhanced by surface water (i.e., hydrofracturing), leading to mechanical failure of the tall ice cliffs that are left behind (DeConto & Pollard, 2016). MICI is only triggered in climates warmer than present and a recent study by DeConto et al. (2021) suggests ice sheet simulations without MICI dynamics fail to reproduce the last interglacial and Pliocene observational constraints on ice loss.

A source of bias in many recent projections of the AIS contribution to GMSL is meltwater expulsion due to the uplifting solid Earth from marine-based sectors of the ice sheet where ice is lost (Figure 1a; e.g., Bamber et al., 2009; Goelzer et al., 2020; Gomez et al., 2010; J. X. Mitrovica et al., 2009; Pan et al., 2021; Powell et al., 2021). Early studies that considered this water expulsion mechanism used elastic or 1-D viscoelastic profiles to simulate the Earth rheology (Bamber et al., 2009; Gomez et al., 2010). The relatively high mantle viscosity values and thick lithosphere adopted in these studies underestimate the rate and magnitude of uplift in regions of the West Antarctic Ice Sheet (WAIS) that are underlain by anomalously low viscosity upper mantle and thinned lithosphere (Barletta et al., 2018; Hay et al., 2017; Kaufmann et al., 2005). Pan et al. (2021), accounted

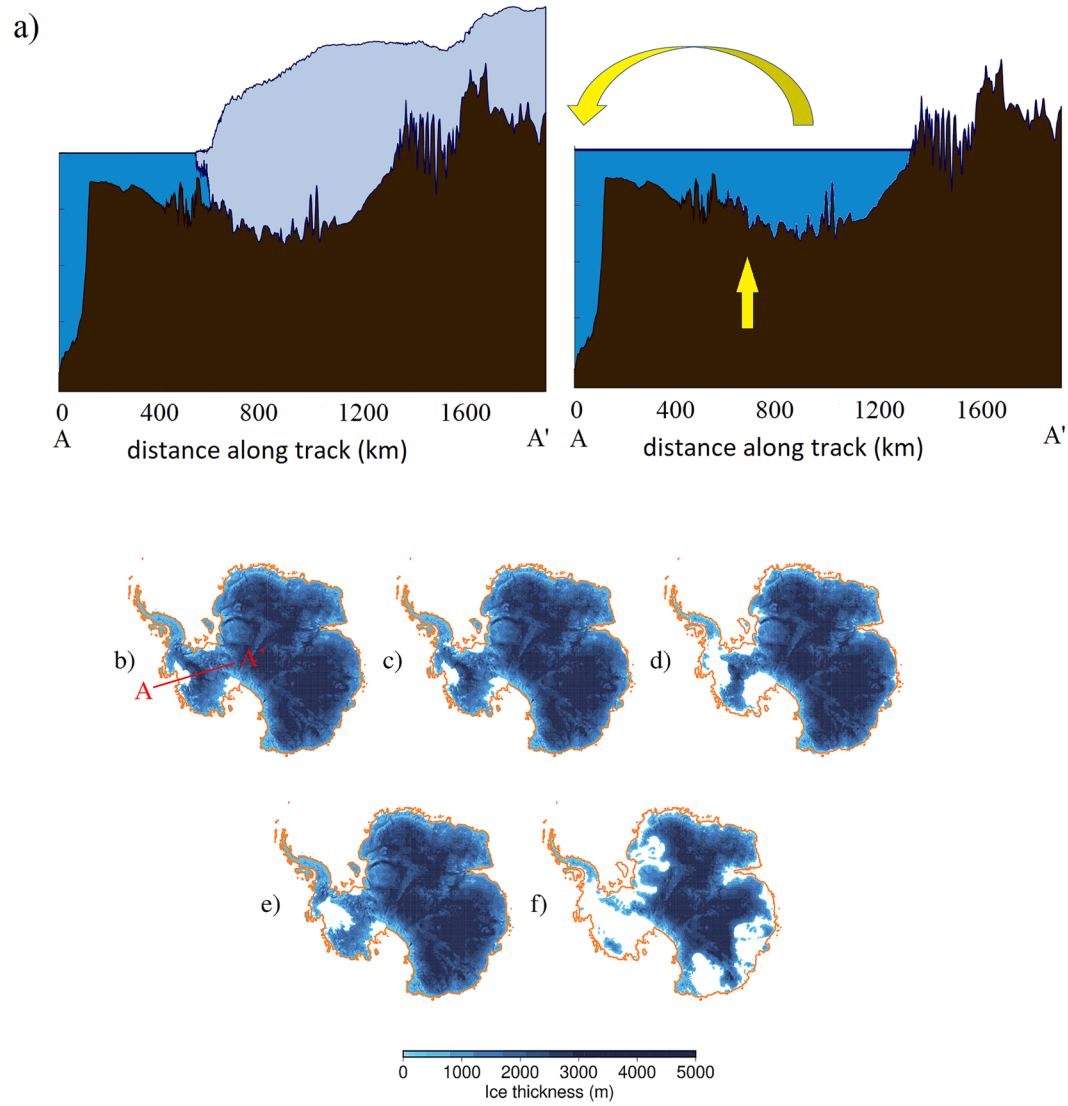

Figure 1. (a) A schematic figure representing the water expulsion process. When marine based ice (left frame) retreats, water fills the accommodation space left behind by the missing ice (right frame). Following the ice loss, the solid Earth beneath the region of ice loss uplifts, reducing the size of the accommodation space and expelling water out into the rest of the global ocean. The profile shown here is an E–W transect in West Antarctic Ice Sheet (Greene et al., 2017) along the profile path (A–A′) as show in panel (b). (b–f) The Ice sheet model projections of Antarctic Ice Sheet at 2500 CE for (b) RCP2.6-MISI, (c) RCP4.5-MISI, (d) RCP8.5-MISI, (e–f) under the emission scenarios of RCP2.6 and RCP8.5, respectively, but including marine ice cliff instability with model physical parameters calibrated using observational constraints (DeConto et al., 2021). The solid orange line marks the grounding line at initial modern (preindustrial) state.

for realistic 3-D heterogeneity in rheological structure in their analysis and found that the water expulsion process amplifies the GMSL change associated with interglacial collapse of marine sectors of the AIS by up to 30% within a rapid (~1 kyr) time scale after ice sheet collapse. The global geometry of the sea-level change associated with the water expelled from uplifting marine section of the AIS is spatiotemporally variable, and notably involves ocean floor subsidence at the periphery regions of WAIS ice loss that acts to compensate for some of the sea-level rise at far-field sites from ongoing expulsion. Pan et al. (2021) also considered one future WAIS collapse scenario and found that water expulsion has the potential to substantially increase the calculated GMSL rise across the 21st century. However, the impact of water expulsion on global sea levels will depend on the geometry and timing of both bedrock deformation and ice sheet retreat in marine sectors, thus an exploration of this effect on future AIS sea-level contributions requires consideration across a range of climate forcing scenarios, ice model physics (i.e., MISI and MICI) and adopted Earth viscosity structures.

In this study, we use a global sea-level model (Latychev et al., 2005) to estimate the contribution of the AIS to sea-level change from 1950 to 2500. Our results focus on both the contribution of the AIS to future GMSL rise, and the global geometry of the associated sea-level change. The AIS evolution is simulated by PSUICE3D model (DeConto et al., 2021) forced by high (RCP8.5), intermediate (RCP4.5) and low (RCP2.6) greenhouse gas emissions and in some cases incorporate MICI ice physics. We quantify the influence of the solid Earth and associated gravitational and Earth rotational effects on the signal of water expulsion mechanism in future sea levels using a suite of Earth structures model.

2. Methods

The GMSL rise due to Antarctic mass loss is calculated by averaging the total amount of sea-level change over the open-ocean area. Here, the open ocean is defined as the ocean area that excludes marine-based sectors in Antarctica. We note that the area of the ocean is fixed to its value at the start of the simulation, as tests showed that incorporating changes in the area of the ocean across the time period of the simulation has negligible effect. We begin by simulating five different representative scenarios of AIS evolution using the PSU ice model (Section 2.1) and then a sea-level model (Section 2.2) uses these ice sheet simulations to estimate the associated global-scale, geographically variable sea-level change. Finally, we compute from these global fields the GMSL rise associated with each scenario.

For comparison, we also provide an alternative "ice-above-floatation" estimate of the GMSL contribution from the AIS that is commonly adopted in ice sheet modeling. This calculation is based on the maximum volume of ice that can be removed before the ice becomes afloat at a given timestep in the simulation, which depends on both the ice thickness and bedrock elevation at that time. This calculation is performed directly in the ice sheet model (i.e., no sea-level model is involved).

2.1. Ice Sheet Simulation

We use the PSUICE3D model (DeConto et al., 2021; Pollard & DeConto, 2012b; Pollard et al., 2015) to predict the geometry of Antarctic mass loss over a period of 550 years with annual temporal resolution. This ice model adopts a heuristic combination of vertically integrated shallow-ice and shallow-shelf approximations to simulate ice dynamics (Pollard & DeConto, 2012a). In comparison to the previous versions (e.g., DeConto & Pollard, 2016), there are several improvements on different aspects of the model including grounding line parameterization, formulations of ice-shelf buttressing, hydrofracturing, and meltwater feedback mechanisms. A simplified elastic lithosphere, relaxed asthenosphere (ELRA) model (Huybrechts and de Wolde, 1999) is used to compute bedrock elevation changes associated with ice loading during the ice sheet model simulations. We note that our analysis does not consider the effects of ongoing GIA associated with global ice mass variations prior to 1950. This signal is highly uncertain (e.g., Whitehouse et al., 2019) and expected to be small compared to the signal associated with ongoing ice loss (e.g., see Larour et al., 2019). For more detail on the model and future simulation set up, the reader is referred to Pollard and DeConto (2012b, 2020) and DeConto et al. (2021), respectively.

The initial ice sheet conditions are set to the modern (preindustrial) state and thus all the simulations begin in 1950 and terminate at 2500. We take the inverse methodology described in Pollard and DeConto (2012a) to determine the initial basal sliding coefficients. The bathymetric boundary conditions such as bedrock elevation and ice surface elevation are adopted from Bedmap2 data set (Fretwell et al., 2013). The grid resolution for all ice sheet simulations is 10 km. Calculations of the annual surface mass balance on the AIS are based on the estimates of precipitation and monthly mean surface air temperatures provided by RegCM3 regional climate model (RCM) adapted to Antarctica (Pal et al., 2007). Ocean temperatures, sea-surface temperature, and sea-ice boundary conditions are derived from National Center for Atmospheric Research (NCAR) CCSM4 simulations. The atmospheric and oceanic forcings follow the extended RCP scenarios: RCP2.6, RCP4.5, and RCP8.5 (Meinshausen et al., 2011).

In all model simulations, we consider MISI dynamics on reverse-sloped bedrock. In two of the five sets of simulations, we additionally incorporate hydrofracturing and mechanical failure of the marine-terminating ice cliffs (MICI) as in DeConto et al. (2021). In the latter, there are two main tunable cliff-calving parameters which are chosen as the average calibrated values constrained to best reproduce last interglacial, Pliocene and modern

observations of ice loss (DeConto et al., 2021). Figures 1b–1f shows the five different scenarios of the modeled grounded ice evolution at the end of the simulations (2500 CE) for RCP emission trajectories (RCP2.6, RCP4.5, and RCP8.5) with and without MICI related processes.

2.2. Sea-Level Model

The calculation of projected sea-level change is based on solving a generalized form of the sea-level equation that is described in detail in Gomez et al. (2010). Two key inputs of this model are the spatial and temporal evolution of the ice (see Section 2.1) and the rheological structure of the Earth in response to ice loading. This sea-level calculator incorporates time-varying migration of shorelines (J. X. Mitrovica & Milne, 2003; Kendall et al., 2005), the influence of load-induced perturbation in Earth rotation (J. X. Mitrovica et al., 2005), and the viscoelastic deformation of a self-gravitating, Maxwell (viscoelastic) Earth (Peltier, 1974).

A finite volume method is adopted in this study to solve the sea-level equation on a global tetrahedral grid with triangulated spherical surfaces (Latychev et al., 2005). Our computational grid consists of ∼28 million grid nodes and ∼160 million elements with ∼7 km surface resolution over Antarctica (12–15 km elsewhere) which decreases with depth to ∼50 km at the core-mantle boundary. The ice thickness derived from PSU ice sheet simulations are projected onto this computational grid at every 2 years. The radial structure of the grid comprises 70 spherical layers separated by distances that are similar to the resolution of these corresponding triangulated surface to ensure relatively regular geometry for the tetrahedrons. This 3-D global sea-level model is used to perform simulations incorporating a range of models of Earth structure, including two 3-D viscoelastic models based on seismic tomography, one 1-D radially varying Earth structure models and a purely elastic Earth model. We describe each Earth structure model in turn below.

We develop a 3-D viscoelastic structure that consists of an outer elastic lithosphere layer with variable thickness on top of the viscous mantle. The lateral variations in lithosphere thickness are based on the global model of Conrad and Lithgow-Bertelloni (2006) combined with the regional model of An et al. (2015a) over Antarctica (Figure S1a in Supporting Information S1). The lithosphere thickness model is scaled to have an average lithosphere thickness of 96 km over Antarctica and a minimum of 40 km, following the work of Hay et al. (2017). The density and elastic structures in all sea-level simulations are radially variable and defined based on the seismic model STW105 (Kustowski et al., 2008).

Two 3-D mantle viscosity structures, which were first constructed in Wan et al. (2022), are built upon two different 1-D reference viscosity profiles:—the first model we referred to as EM3D_L, is characterized by a uniform viscosity of 10^{20} Pa s in the upper mantle (from the bottom of the lithosphere to the depth of 670 km), and a viscosity value of 5×10^{21} Pa s within the lower mantle (from 670 km depth to the core-mantle boundary);—the second model, EM3D_M, adopts the same reference viscosity within the lower mantle, but has higher background viscosity of 5×10^{20} Pa s in the upper mantle (Figure S1b in Supporting Information S1). The variations in viscosity relative to the assumed reference model are derived by first combining the ANT-20 regional shear-wave seismic velocity model of the upper mantle beneath Antarctica (Lloyd et al., 2020) with the S362ANI global seismic tomography model (Kustowski et al., 2008). The S362ANI model has a resolution on order of 1,000 km. The ANT-20 model is a state-of-the-art regional model that resolves structures with a spatial scale of order ∼100 km between 50 and 410 km depths and higher values at greater depths. For a detailed description of the construction of the 3-D viscosity models see Section S1 in Supporting Information S1.

As discussed earlier in this section, the computational set up of the elastic and the 1-D viscoelastic models are the same as the 3-D models, except that there is no viscous deformation (i.e., the viscosity is set to be very high throughout the Earth) in the elastic case. To construct the 1-D viscoelastic model, we adopt constant upper and lower mantle viscosities of 10^{20} Pa s and 5×10^{21} Pa s, respectively. The elastic thickness of the lithosphere is set to the global average value of the 3-D lithosphere thickness model, that is, 96 km.

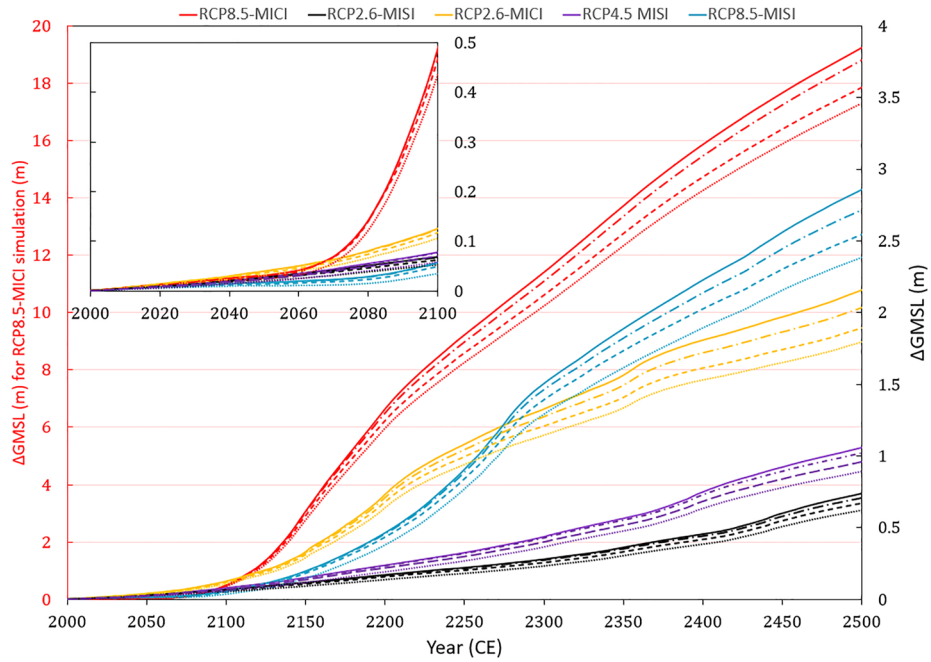

Figure 2. Contribution of Antarctica to future global mean sea-level (GMSL) rise calculated from the five ice histories shown in Figures 1b–1f and different assumptions of solid Earth deformation and water expulsion. Solid lines show the results generated based on the EM3D_L model including the water expulsion process. Dash-dotted lines show model results in which lateral variability in the Earth structure is not included, that is, a 1-D viscoelastic Earth model is adopted (upper mantle viscosity of 10^{20} Pa s, lower mantle viscosity of 5×10^{21} Pa s, and lithosphere thickness of 96 km; see Section 2.2) but the water expulsion mechanism is considered. Dotted lines represent the GMSL estimates calculated from the "ice-above-floatation" method in the PSU ice sheet/shelf model, which simulates the bedrock motions using the elastic lithosphere, relaxed asthenosphere deformation model. Dashed lines are associated with the case using the same 3-D structure but without considering the water expulsion mechanism. For the purpose of clarity, the red curves (RCP8.5-MICI) are shown using the left vertical axis and those related to the rest of the models are shown using the right vertical axis. The inset shows the results until the end of the 21st century.

3. Results and Discussion

3.1. Future GMSL Projections

Figure 2 shows the projected contribution of the AIS to future GMSL rise based on the different melt geometries shown in Figures 1b–1f during the time period 2000–2500 CE, where the solid lines are calculations that incorporate 3-D Earth structure and the water expulsion mechanism (Figure 1a). There is a large spread in the predicted future Antarctic contributions and various patterns of the GMSL rate change (Figure S2a in Supporting Information S1), ranging from 0.74 m (RCP2.6-MISI; solid black line in Figure 2, with amplitude given by the right ordinate axis) to ~19.2 m (RCP8.5-MICI; solid red line in Figure 2, with amplitude given by the left ordinate axis) by 2500. At 2100, both simulations with MICI produce higher values (0.12 and 0.48 m for RCP2.6 and RCP8.5 scenarios, respectively) in comparison to models without this process (0.07 and 0.06 m for RCP2.6 and RCP8.5). The warming climate triggers increased precipitation and causes net ice mass gain over East Antarctic Ice Sheet (EAIS) in all scenarios except RCP8.5-MICI, which partly compensate for the ice loss in West Antarctica and Antarctic Peninsula. With RCP8.5-MICI, substantial retreat of marine basins in East Antarctica due to cliff failure dominates over the interior mass gain. The results associated with the intermediate scenario (RCP4.5-MISI) lies within the minimum and maximum bounds with GMSL values of 0.08 and 1.06 m at 2100 and 2500, respectively.

The dashed lines in Figure 2 represent calculations that do not permit water expulsion from the uplifting marine-based sectors. The difference between results with and without water expulsion ranges from ~4% (RCP8.5-MICI, 0.02 m) to ~16% (RCP8.5-MISI, ~0.01 m) at 2100% and 7% (RCP8.5-MICI, 1.4 m) to 14% (RCP2.6-MICI, 0.26 m) at the end of the simulations (see also Figure S2b in Supporting Information S1). Our findings are generally consistent with the results of Pan et al. (2021), who considered a simulation similar to

our RCP8.5-MISI simulation but with applying a different 3-D Earth mode and over a longer time period and suggested that the water expulsion mechanism would add up to 18% and 19% to the GMSL rise estimates by 2100 and 2850 CE, respectively. In absolute terms, the contribution from water expulsion scales, approximately, with the ice mass flux, so that the RCP8.5-MICI simulation yields a contribution of ∼1.4 m at 2500 CE, while this number drops to 0.07 m, 0.09 m, 0.26 m, and 0.30 m for the RCP2.6-MISI, RCP4.5-MISI, RCP2.6-MICI, and RCP8.5-MISI scenarios, respectively.

The dash-dotted curves represent the GMSL calculations based on the 1-D viscoelastic Earth model. The impact of lateral variations in mantle viscosity and lithospheric thickness on GMSL predictions is relatively small, such that ignoring this structure leads to an underestimate of the amplitude of the GMSL rise by up to 3.5% at 2100 and 6% at 2500 for RCP2.6-MICI simulation.

The "ice-above-floatation" GMSL estimates from the ice sheet model (see Section 2.1) are shown in Figure 2 as dotted lines. GMSL calculations with this method are underestimated by 12% (RCP8.5-MICI) to 64% (RCP8.5-MISI) at the end of the 21st century and ∼11% (RCP8.5-MICI) to 20% (RCP2.6-MICI) at the end of the simulations. There are two assumptions that are responsible for this discrepancy. First, the bedrock elevation changes in the ice sheet simulation are modeled using the standard ELRA method characterized by an elastic lithosphere on top of a relaxing asthenosphere with a single decay time of 3,000 years, resulting in less deformation during the 500-year simulation than predicted with the sea-level model based on 3-D Earth structure with weaker mantle viscosities and thinner lithosphere in much of the WAIS. Second, the model does not account for water expulsion and only considers the areas that remain covered by ice in the ice-above-floatation calculation, which produces systematically lower predicted GMSL values. The limitation of this approach in ice sheet models has been discussed in recent studies (e.g., Adhikari et al., 2020; Goelzer et al., 2020; Pan et al., 2021). Differences between the estimate based on ice-above-floatation with the ELRA model and the 1-D viscoelastic model are more due to the different methods of performing the calculation, but the different formulation of Earth deformation with these two approaches also contributes.

3.2. The Sensitivity to the Adopted Earth Structure

Next, we explore the influence of the adopted Earth structure on results by comparing simulations with elastic, 1-D viscoelastic and 3-D viscoelastic Earth models. Figures 3a and 3b show the effect of considering a purely elastic Earth model relative to the 3-D viscoelastic case on the sea-level model predictions for the RCP8.5-MISI scenario. All model simulations include the water expulsion process. The differences in the far-field are small ($<\pm$0.3 m for a GMSL value of ∼2.9 m), in agreement with Powell et al. (2021). However, closer to the marine sectors of the WAIS, in comparison to a purely elastic model, a viscoelastic model predicts larger amplitude of sea-level fall beneath and around the zone of ice loss (up to ∼120 m), red regions in Figures 3b and 3a zone of sea-level rise on the peripheral regions (up to ∼40 m), blue regions in Figure 3b, that are subsiding due to the viscous flow of the mantle toward uplifting regions upon deglaciation. This agrees with the results of Hay et al. (2017), who explored the sensitivity of the predicted sea-level fingerprints to variability in the Earth structure.

The relatively low sensitivity of far-field sea-level predictions to the adopted Earth model arises because the lateral heterogeneity in Earth structure impacts both the water expulsion process and a mechanism termed ocean syphoning (J. X. Mitrovica and Milne, 2002; J. X. Mitrovica and Peltier, 1991). Syphoning refers to the drawing of water away from the far field toward accommodation space created by subsiding peripheral bulges. The weak upper mantle viscosity beneath and around the Western Antarctica in the 3-D Earth model (Figure S1b in Supporting Information S1) leads to local viscous adjustment with relatively shorter viscoelastic relaxation time. This rapid adjustment acts to accentuate the water expulsion mechanism, but it also amplifies ocean syphoning by amplifying the collapse of the peripheral bulge offshore Antarctic. The two effects partly compensate for each other in their impact on far field sea level.

While in the elastic case the water expelled from marine sectors is distributed across the far-field region outside of the zone of sea-level fall, with a viscoelastic Earth model the near-field subsided peripheral bulges capture some of the expelled water from the rebounding inundated marine-based sectors (Pan et al., 2021). In order to determine an approximate amount of water that is delivered to the far-field ocean basins, we averaged the differential global sea level across the open ocean area covering latitudes higher than 40°S to avoid bulge dynamics that

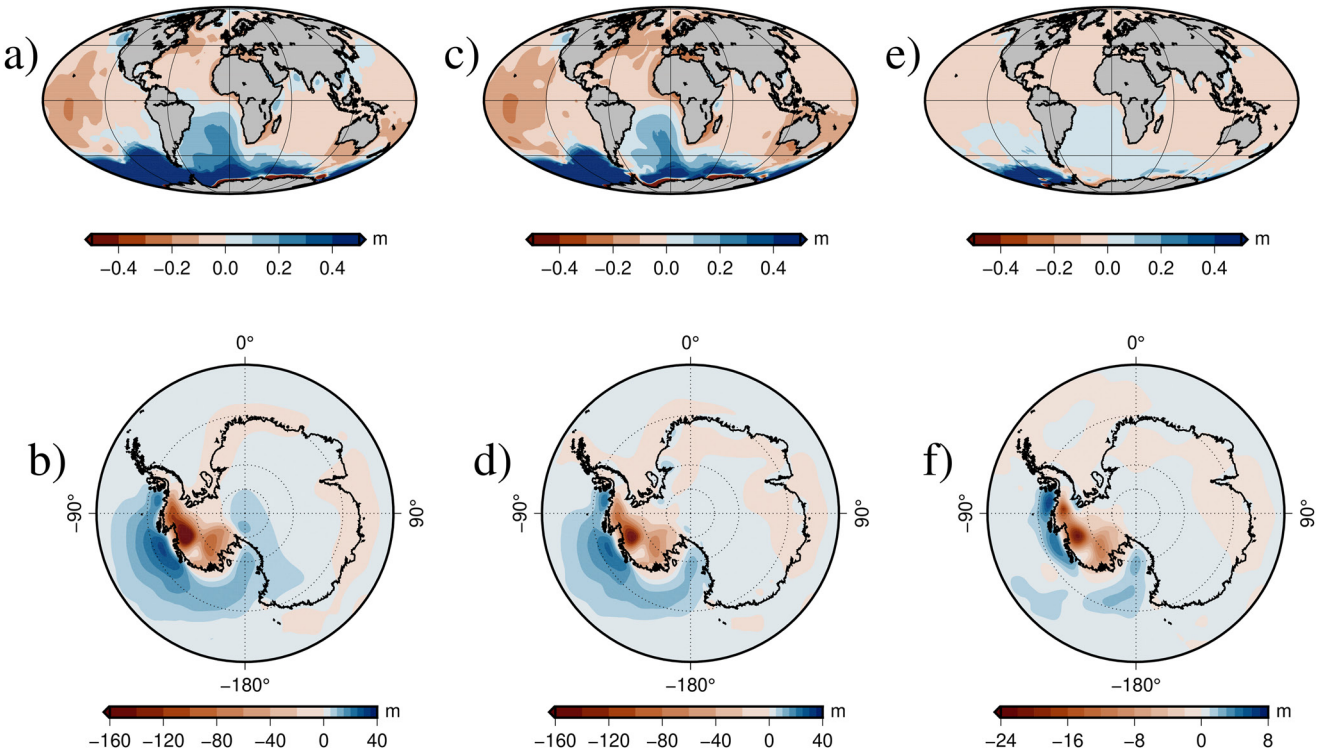

Figure 3. Sensitivity of the model predictions to the applied Earth structure. The difference between projected sea-level change at the end of simulations (2500 CE) assuming RCP8.5-MISI ice loading and Earth model EM3D_L and (a) a purely elastic Earth model (EM3D_L minus elastic), (c) the reference 1-D Earth model (EM3D_L minus 1-D), (e) EM3D_M model (EM3D_L minus EM3D_M), (b, d, f) similar to (a, c, e) but with a regional Antarctic view. Note the different scale in frame (f).

extend to the southern tip of South America. The results suggest that ∼84% of the expelled meltwater is transported to the far-field oceans in the viscoelastic case (this percentage drops by ∼4% from 2100 to 2500 owing to the subsidence of the peripheral bulges), compared to 91% in the elastic case.

Figures 3c and 3d show the difference between the predicted model results for the RCP8.5-MISI ice model at 2500 CE inferred from the EM3D_L and the reference 1-D Earth model. The spatial distribution and amplitude of the sea-level changes obtained from the 1-D model is similar to that of the elastic case (Figures 3a and 3b). We also perform an additional sensitivity analysis by adopting the second 3-D viscoelastic model EM3D_M (Figures 3e and 3f). The difference between the results obtained using this Earth model relative to the EM3D_L model is negligible in the far field (<0.1 m or ∼3% of the global average value) and suggests moderately lower sea-level rise (∼7 m) offshore zone of West Antarctica. The latter discrepancy is due to the faster viscoelastic response of the EM3D_L model due to its lower viscosity (Figure S1b in Supporting Information S1) which leads to higher amplitude peripheral subsidence of the crust and sea-level rise.

Finally, we note that although neglecting lateral variations in Earth structure introduces a moderate error in GMSL projections—that is, the 3-D and 1-D models we have adopted yield similar integrated changes in sea level—a recent study has emphasized that the local error in interglacial sea-level predictions introduced by neglecting lateral viscosity variations is a considerable fraction of the total GIA-derived (geographically variable) signal (Powell et al., 2021). Our predictions support this argument—calculations that include such structure are characterized by a maximum difference of ∼66% in the South Pacific Ocean (calculated relative to the 3-D minus 1-D sea-level change integrated across the surface area north of 50°S) and ∼22% in far-field (integrated over open ocean north of 40°S) relative to predictions of sea-level change based on 1-D Earth models (Figure S3 in Supporting Information S1). We note that the overall results obtained in our study holds for the range of considered ice scenarios (not shown). For the case of more intense ice melt from East and West Antarctica with MICI (RCP8.5-MICI, Figure S4 in Supporting Information S1), the discrepancy between model results considering

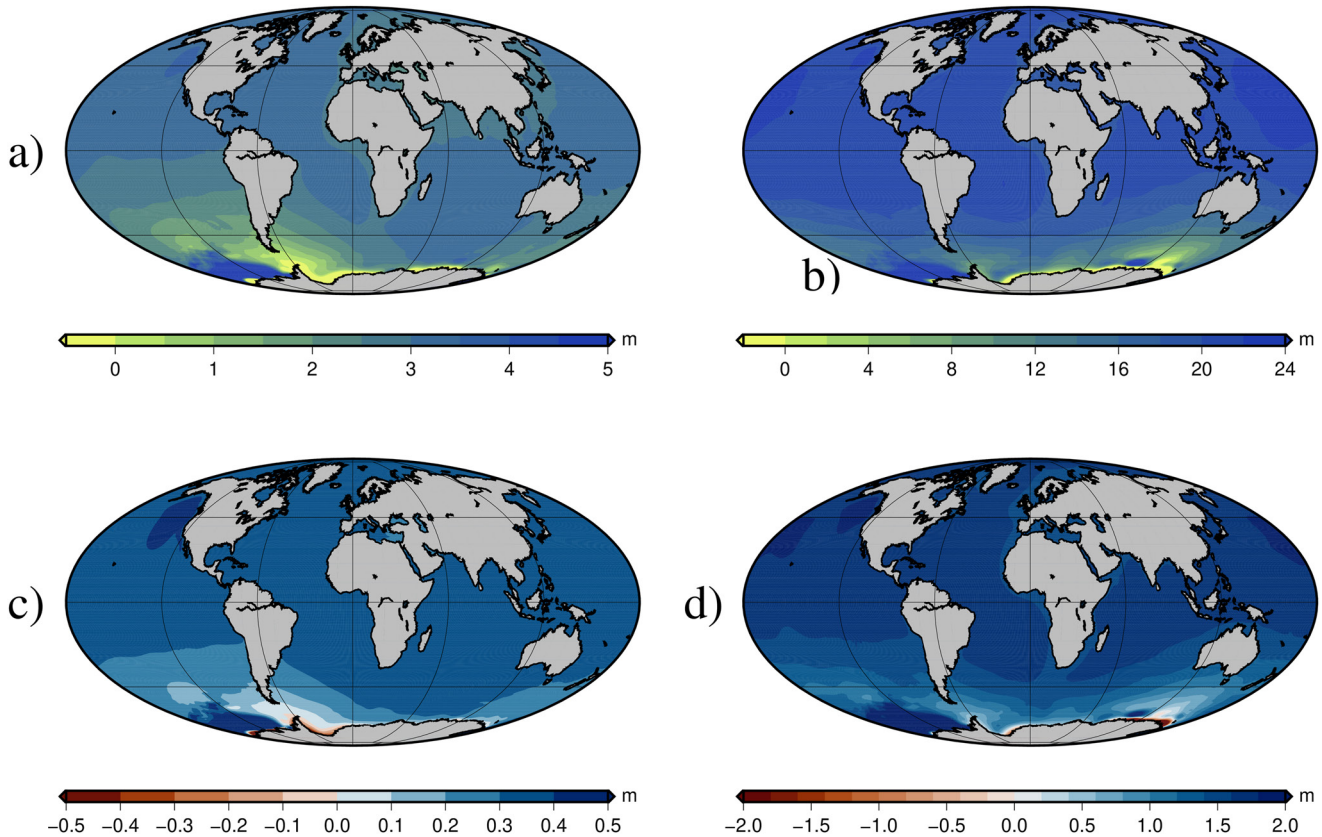

Figure 4. The influence of the water expulsion mechanism on the spatial distribution of projected sea-level change. Change in global sea level at 2500 CE relative to 2000 CE associated with different Antarctic Ice Sheet evolution scenarios: (a) RCP8.5-MISI and (b) RCP8.5-MICI shown in Figures 1d and 1f, respectively. Simulations include the effect of water expulsion and adopt the EM3D_L model. (c–d) The difference between simulations that include water expulsion (i.e., figures a, b) and the corresponding simulations in which the water expulsion mechanism is not included (expulsion minus no expulsion).

different Earth structures show greater amplitude far away from the melting zone reaching its peak values at ∼1.6 and −3 m, equivalent to 8% and ∼16% of the GMSL, over the Red Sea and Iceland, respectively.

3.3. The Impact of Water Expulsion on Global Sea-Level Distribution

We next consider projections of the geographical distribution of the Antarctic meltwater and the impact of water expulsion on this distribution. Figures 4a and 4b shows the sea-level change associated with AIS ice loss at 2500 following the RCP8.5 emission scenario with MISI-only (Figure 1d) and with MICI (Figure 1f). The models associated with these results incorporate EM3D_L viscosity model and include water expulsion. In the near field regions for the MISI retreat scenario (Figure 4a), reduced ice-ocean gravity associated with the ice loss causes sea-level to fall by up to ∼145 m (deep yellow zone), while crustal subsidence at the periphery of the WAIS results in a peak sea-level rise of ∼22 m (dark blue zone; note that in both cases the color bar is saturated to allow for better visualization of the global sea-level distribution). We note that a small portion (up to 2–3 m) of the sea-level rise around the peripheral bulges is due to the water expulsion effect. This pattern of sea-level fall and rise due to the gravitational loss and peripheral bulge subsidence also occurs around the EAIS, but the amplitude is smaller in comparison to WAIS. At greater distances from the ice loss, sea level progressively rises with peak values of 3.67 and 3.45 m along the western coastline of North America and in the Indian Ocean, respectively. The enhanced sea-level rise in these two regions is consistent with previous studies and driven by the effect of the southern rotation axis moving toward the zone of ice loss in West Antarctica (e.g., Gomez et al., 2010; Hay et al., 2017; Pan et al., 2021).

In the case of the MICI simulation (Figure 4b), the geometry of the sea-level change follows a similar pattern to that of MISI, but with higher amplitudes due to the additional contribution from EAIS meltwater. For example,

the localized sea-level fall and rise in the near-field zone of Wilkes Land in East Antarctica reaches 160 and 43 m, respectively, due to significant EAIS retreat in this scenario. Far-field peaks reach ~22 m in the northwest Pacific Ocean and the south Atlantic, where the change in location of the peaks relative to the RCP8.5-MISI scenario is due to significant ice loss originating from the EAIS which drives motion of the southern rotation axis toward the opposite direction.

In Figures 4c and 4d we quantify the influence of water expulsion from uplifted marine sectors of the AIS on geographically variable global sea-level change for the two ice retreat scenarios considered above. Water expulsion contributes a sea-level rise across the far-field that reaches a maximum of 0.43 m (~11% of the total signal) for MISI and 1.89 m (~9%) for MICI in the northwest Pacific Ocean. In the near field, uplift beneath marine sections and associated unloading due to water expulsion amplifies sea-level rise up to 2.1 m (10%) for MISI and 7.8 m (14%) for MICI, respectively. In Figures S5a–S5d in Supporting Information S1 we present analogous plots to Figures 4a–4d for RCP2.6 scenario at 2500. These show similar results albeit with different amplitude, for example, the effect of the water expulsion in the far-field is 0.09 m (10%) in case of MISI and 0.34 m (12%) for MICI. Note that the impact of the water expulsion in absolute terms varies through time and in general increases toward the end of the simulations (see Figure S2a in Supporting Information S1).

4. Conclusions

We have tracked geographically variable sea-level change and GMSL rise to 2500 CE in an ice age sea-level model to quantify the signal from water expulsion and determine the sensitivity to assumptions made regarding viscoelastic Earth structure. The calculations are based on simulations of AIS mass loss considering different climate forcings (RCP2.6 and RCP8.5) and ice physics (with and without MICI). Our calculations of GMSL range from 0.06 to 0.48 m at the end of the 21st century and 0.74–19.2 m at 2500. We find that the contribution of water expulsion varies for the different ice loss scenarios, ranging from 4% to 16% at 2100 and 7%–14% at 2500. Our results also suggest that using the simple ELRA-bed model and the ice-above-floatation GMSL procedure applied in most ice sheet models, underestimate the GMSL predictions by 12%–64% at 2100 and 11%–20% at 2500. The influence of incorporating lateral variability in viscosity structure on GMSL projection is relatively small, however, this signal is significantly greater for predictions of geographically variable sea-level change.

Data Availability Statement

All model results produced in this study are available through the following link: https://datadryad.org/stash/share/Zgxv_caT-dpJFY4mS9rFutjiQI-MQDefD5AvgZwlHc4.

Acknowledgments
We thank the anonymous reviewers for their constructive reviews. Maryam Yousefi, Jannette Wann and Natalya Gomez were supported by the Natural Sciences and Engineering Research Council of Canada (Grant No. RGPIN-2016-05159) and the Canada Research Chairs program (Grant No. 241814). This work was also supported by the National Science Foundation (NSF), grants 174490, 1745074, 1744852, and 1744889. Computational resources were provided by Compute Canada and the Canadian Foundation for Innovation. Linda Pan was supported by the Fonds de Recherche du Québec–Nature et technologies, Natural Sciences and Engineering Research Council of Canada, and Star-Friedman Challenge of Harvard University.

References

Adhikari, S., Ivins, E. R., Larour, E., Caron, L., & Seroussi, H. (2020). A kinematic formalism for tracking ice–ocean mass exchange on the Earth's surface and estimating sea-level change. *The Cryosphere*, *14*(9), 2819–2833. https://doi.org/10.5194/tc-14-2819-2020

An, M., Wiens, D. A., Zhao, Y., Feng, M., Nyblade, A. A., Kanao, M., et al. (2015). S-velocity model and inferred Moho topography beneath the Antarctic Plate from Rayleigh waves. *Journal of Geophysical Research: Solid Earth*, *120*(1), 359–383. https://doi.org/10.1002/2014JB011332

Bamber, J. L., Riva, R. E. M., Vermeersen, B. L. A., & LeBrocq, A. M. (2009). Reassessment of the potential sea-level rise from a collapse of the West Antarctic Ice Sheet. *Science*, *324*(5929), 901–903. https://doi.org/10.1126/science.1169335

Barletta, V. R., Bevis, M., Smith, B. E., Wilson, T., Brown, A., Bordoni, A., et al. (2018). Observed rapid bedrock uplift in Amundsen Sea embayment promotes ice-sheet stability. *Science*, *360*(6395), 1335–1339. https://doi.org/10.1126/science.aao1447

Conrad, C. P., & Lithgow-Bertelloni, C. (2006). Influence of continental roots and asthenosphere on plate-mantle coupling. *Geophysical Research Letters*, *33*(5), L05312. https://doi.org/10.1029/2005gl025621

DeConto, R. M., & Pollard, D. (2016). Contribution of Antarctica to past and future sea-level rise. *Nature*, *531*(7596), 591–597. https://doi.org/10.1038/nature17145

DeConto, R. M., Pollard, D., Alley, R. B., Velicogna, I., Gasson, E., Gomez, N., et al. (2021). The Paris Climate Agreement and future sea-level rise from Antarctica. *Nature*, *593*(7857), 83–89. https://doi.org/10.1038/s41586-021-03427-0

Fretwell, P., Pritchard, H. D., Vaughan, D. G., Bamber, J. L., Barrand, N. E., Bell, R., et al. (2013). Bedmap2: Improved ice bed, surface and thickness datasets for Antarctica. *The Cryosphere*, *7*(1), 375–393. https://doi.org/10.5194/tc-7-375-2013

Goelzer, H., Coulon, V., Pattyn, F., de Boer, B., & van de Wal, R. (2020). Brief communication: On calculating the sea-level contribution in marine ice-sheet models. *The Cryosphere*, *14*(3), 833–840. https://doi.org/10.5194/tc-14-833-2020

Gomez, N., Mitrovica, J. X., Tamisiea, M. E., & Clark, P. U. (2010). A new projection of sea level change in response to collapse of marine sectors of the Antarctic ice sheet. *Geophysical Journal International*, *180*(2), 623–634. https://doi.org/10.1111/j.1365-246X.2009.04419.x

Greene, C. A., Gwyther, D. E., & Blankenship, D. D. (2017). Antarctic Mapping tools for MATLAB. *Computers & Geosciences*, *104*, 151–157. https://doi.org/10.1016/j.cageo.2016.08.003

Hay, C. C., Lau, H. C., Gomez, N., Austermann, J., Powell, E., Mitrovica, J. X., et al. (2017). Sea level fingerprints in a region of complex Earth structure: The case of WAIS. *Journal of Climate*, *30*(6), 1881–1892. https://doi.org/10.1175/JCLI-D-16-0388.1

Huybrechts, P., & de Wolde, J. (1999). The dynamic response of the Greenland and Antarctic ice sheets to multiple-century climatic warming. *Journal of Climate*, *12*(8), 2169–2188. https://doi.org/10.1175/1520-0442(1999)012<2169:tdrotg>2.0.co;2

Kaufmann, G., Wu, P., & Ivins, E. R. (2005). Lateral viscosity variations beneath Antarctica and their implications on regional rebound motions and seismotectonics. *Journal of Geodynamics*, *39*(2), 165–181. https://doi.org/10.1016/j.jog.2004.08.009

Kendall, R. A., Mitrovica, J. X., & Milne, G. A. (2005). On post-glacial sea level—II. Numerical formulation and comparative results on spherically symmetric models. *Geophysical Journal International*, *161*(3), 679–706. https://doi.org/10.1111/j.1365-246x.2005.02553.x

Kustowski, B., Ekstrom, G., & Dziewoński, A. (2008). Anisotropic shear-wave velocity structure of the Earth's mantle: A global model. *Journal of Geophysical Research*, *113*(B6), B06306. https://doi.org/10.1029/2007JB005169

Larour, E., Seroussi, H., Adhikari, S., Ivins, E., Caron, L., Morlighem, M., & Schlegel, N. (2019). Slowdown in Antarctic mass loss from solid Earth and sea-level feedbacks. *Science*, *364*(6444), eaav7908. https://doi.org/10.1126/science.aav7908

Latychev, K., Mitrovica, J. X., Tromp, J., Tamisiea, M., Komatitsch, D., & Christara, C. (2005). Glacial isostatic adjustment on 3D Earth models: A finite-volume formulation. *Geophysical Journal International*, *161*(2), 421–444. https://doi.org/10.1111/j.1365-246X.2005.02536.x

Lloyd, A. J., Wiens, D. A., Zhu, H., Tromp, J., Nyblade, A. A., Aster, R. C., et al. (2020). Seismic structure of the Antarctic upper mantle imaged with adjoint tomography. *Journal of Geophysical Research: Solid Earth*, *125*(3), B017823. https://doi.org/10.1029/2019JB017823

Meinshausen, M., Smith, S. J., Calvin, K., Daniel, J. S., Kainuma, M. L. T., Lamarque, J.-F., et al. (2011). The RCP greenhouse gas concentrations and their extensions from 1765 to 2300. *Climatic Change*, *109*(1–2), 213–241. https://doi.org/10.1007/s10584-011-0156-z

Mitrovica, J. X., Gomez, N., & Clark, P. U. (2009). The sea-level fingerprint of West Antarctic collapse. *Science*, *323*(5915), 753. https://doi.org/10.1126/science.1166510

Mitrovica, J. X., & Milne, G. A. (2002). On the origin of late Holocene sea-level highstands within equatorial ocean basins. *Quaternary Science Reviews*, *21*(20–22), 2179–2190. https://doi.org/10.1016/s0277-3791(02)00080-x

Mitrovica, J. X., & Milne, G. A. (2003). On post-glacial sea level: I. General theory. *Geophysical Journal International*, *154*(2), 253–267. https://doi.org/10.1046/j.1365-246x.2003.01942.x

Mitrovica, J. X., & Peltier, W. R. (1991). On postglacial geoid subsidence over the equatorial oceans. *Journal of Geophysical Research*, *96*(B12), 20053–20071. https://doi.org/10.1029/91JB01284

Mitrovica, J. X., Wahr, J., Matsuyama, I., & Paulson, A. (2005). The rotational stability of an ice age Earth. *Geophysical Journal International*, *161*(2), 491–506. https://doi.org/10.1111/j.1365-246x.2005.02609.x

Morlighem, M., Rignot, E., Binder, T., Blankenship, D., Drews, R., Eagles, G., et al. (2019). Deep glacial troughs and stabilizing ridges unveiled beneath the margins of the Antarctic ice sheet. *Nature Geoscience*, *13*(2), 132–137. https://doi.org/10.1038/s41561-019-0510-8

Pal, J. S., Giorgi, F., Bi, X., Elguindi, N., Solmon, F., Rauscher, S. A., et al. (2007). Regional climate modeling for the developing world: The ICTP RegCM3 and RegCNET. *Bulletin of the American Meteorological Society*, *88*(9), 1395–1409. https://doi.org/10.1175/BAMS-88-9-1395

Pan, L., Powell, E. M., Latychev, K., Mitrovica, J. X., Creveling, J. R., Gomez, N., & Clark, P. U. (2021). Rapid postglacial rebound amplifies global sea level rise following West Antarctic Ice Sheet collapse. *Science Advances*, *367*(18), eabf7787. https://doi.org/10.1126/sciadv.abf7787

Pattyn, F., & Morlighem, M. (2020). The uncertain future of the Antarctic ice sheet. *Science*, *367*(6282), 1331–1335. https://doi.org/10.1126/science.aaz5487

Peltier, W. R. (1974). The impulse response of a Maxwell Earth. *Reviews of Geophysics*, *12*(4), 649–669. https://doi.org/10.1029/rg012i004p00649

Pollard, D., Chang, W., Haran, M., Applegate, P., & DeConto, R. (2015). Large ensemble modeling of last deglacial retreat of the west Antarctic ice sheet: Comparison of simple and advanced statistical techniques. *Geoscientific Model Development Discussions*, *8*, 9925–9963.

Pollard, D., & DeConto, R. M. (2012a). A simple inverse method for the distribution of basal sliding coefficients under ice sheets, applied to Antarctica. *The Cryosphere*, *6*(5), 953–971. https://doi.org/10.5194/tc-6-953-2012

Pollard, D., & DeConto, R. M. (2012b). Description of a hybrid ice sheet-shelf model, and application to Antarctica. *Geoscientific Model Development*, *5*, 1273–1295. https://doi.org/10.5194/gmd-5-1273-2012

Pollard, D., & DeConto, R. M. (2020). Continuous simulations over the last 40 million years with a coupled Antarctic ice sheet-sediment model. *Palaeogeogaphy, Palaeoclimatology, Palaeoecology*, *537*, 109374. https://doi.org/10.1016/j.palaeo.2019.109374

Powell, E. M., Pan, L., Hoggard, M. J., Latychev, K., Gomez, N., Austermann, J., & Mitrovica, J. X. (2021). The impact of 3-D Earth structure on far-field sea level following interglacial West Antarctic Ice Sheet collapse. *Quaternary Science Reviews*, *273*(107256). https://doi.org/10.1016/j.quascirev.2021.107256

Schoof, C. (2007). Ice sheet grounding line dynamics: Steady states, stability, and hysteresis. *Journal of Geophysical Research*, *112*(F3), 03S28. https://doi.org/10.1029/2006JF000664

Seroussi, H., Nowicki, S., Payne, A., Goelzer, H., Lipscomb, W., Abe Ouchi, A., et al. (2020). ISMIP6 Antarctica: A multi-model ensemble of the Antarctic ice sheet evolution over the 21st century. *The Cryosphere Discussions*, *14*(January), 3033–3070.

Wan, J. X., Gomez, N., Latychev, K., & Han, H. (2022). Resolving GIA in response to modern and future ice loss at marine grounding lines in West Antarctica [Dataset]. Journal of Climate. https://tc.copernicus.org/articles/16/2203/2022/

Whitehouse, P. L., Gomez, N., King, M. A., & Wiens, D. A. (2019). Solid Earth change and the evolution of the Antarctic ice sheet. *Nature Communications*, *10*(1), 503. https://doi.org/10.1038/s41467-018-08068-y

References From the Supporting Information

Nield, G. A., Barletta, V. R., Bordoni, A., King, M. A., Whitehouse, P. L., Clarke, P. J., et al. (2014). Rapid bedrock uplift in the Antarctic Peninsula explained by viscoelastic response to recent ice unloading. *Earth and Planetary Science Letters*, *397*, 32–41. https://doi.org/10.1016/j.epsl.2014.04.019

Zhao, C., King, M. A., Watson, C. S., Barletta, V. R., Bordoni, A., Dell, M., & Whitehouse, P. L. (2017). Rapid ice unloading in the Fleming Glacier region, southern Antarctic Peninsula, and its effect on bedrock uplift rates. *Earth and Planetary Science Letters*, *473*, 164–176. https://doi.org/10.1016/j.epsl.2017.06.002